MATHEMATICAL MODELLING AND NUMERICAL ANALYSIS OF WAVE PROCESSES IN ELASTIC SHELLS

Yuliia Meish[1]
Halyna Isaienko[2]

DOI: https://doi.org/10.30525/978-9934-26-715-4-57

Abstract. The purpose of this chapter is to examine the mathematical modelling and numerical analysis of transient wave processes in elastic shells of variable thickness, with particular reference to truncated conical shells. The study addresses the relationship between model assumptions, numerical approximation and the interpretation of displacement and strain distributions. *Methodology.* A variational formulation is presented for linear axisymmetric shell deformation, incorporating membrane and bending stiffness, transverse shear, translational and rotary inertia, and an optional Winkler foundation. Spatial variations in thickness are retained in the stiffness and inertia coefficients. The additional kinematic fields required to describe nonaxisymmetric deformation are specified. The finite-difference approximation and explicit central-difference integration scheme are examined with regard to spectral stability and spatial and temporal refinement. *Results.* Analysis of the numerical evidence [1] indicates satisfactory agreement between numerical and analytical deflection profiles for the constant-thickness benchmark. Meridional mesh refinement produces stabilisation of selected displacement and stress maxima, whereas temporal refinement reveals differences in convergence between individual strain components. For the fully clamped panels of equal mass considered, the difference between displacement maxima is approximately 25%; these maxima occur at different times. This comparison therefore characterises peak displacements within the examined interval and does not establish

[1] Doctor of Technical Sciences, Professor,
Head of the Department of Higher and Applied Mathematics,
National University of Life and Environmental Sciences of Ukraine, Ukraine
[2] Candidate of Physical and Mathematical Sciences, Associate Professor,
Associate Professor at the Department of Fundamental Disciplines,
Heroes of Kruty Military Institute of Telecommunications and Information Technologies, Ukraine

© Yuliia Meish, Halyna Isaienko

an equivalent reduction in strain or stress. The influence of the elastic foundation becomes more pronounced at later observation times. *Practical implications.* Assessment of thickness distributions requires a specified deformation measure, observation interval and verification procedure. Displacement convergence alone is insufficient to establish stress accuracy. The Winkler foundation represents elastic restraint without introducing damping. Application of the formulation is restricted by the assumptions of linear elasticity and small rotations. The distinction between axisymmetric shell motion and nonaxisymmetric panel deformation defines the scope of the formulation and interpretation of the numerical examples. *Value/ originality.* The chapter refines the mathematical interpretation of variable-thickness effects on the transient deformation of conical shells through the combined consideration of spatially varying stiffness and inertia. It clarifies the comparison of equal-mass shells in terms of peak displacement and its occurrence time, and distinguishes the stability conditions of explicit time integration from the refinement criteria used to assess numerical accuracy.

INTRODUCTION

A load acting over a finite time interval produces a spatially and temporally varying response in an elastic shell. The mathematical problem is to determine the coupled displacement, strain and stress fields while retaining the effects of curvature, local stiffness, inertia and edge restraint. In conical shells, the radius changes along the meridian; when the thickness also varies, both geometry and mechanical coefficients depend on position. These features make the conical shell a useful setting for studying how a continuous initial boundary value problem is represented by a numerical scheme and how the computed transient response should be interpreted [1; 2].

Thickness variation constitutes geometric inhomogeneity even when the material itself is homogeneous. Within the linear shell model adopted here, membrane stiffness and translational inertia depend linearly on thickness, whereas bending stiffness and rotary inertia involve its cube. Consequently, replacing a variable thickness by a constant value does not preserve all mechanical characteristics simultaneously. An equal-mass comparison is particularly informative: it isolates the consequences of redistributing material while keeping the total material quantity fixed.

The selected calculations from the source monograph provide examples of this comparison, alongside cases with different edge restraints and an elastic foundation [1].

The theoretical background is established in the survey of inhomogeneous shell systems under nonstationary loading by Lugovoi and Meish [2] and in the monograph by Luhovyi, Meish V. and Meish Yu. [1]. The conical-shell formulations and numerical examples in [1] provide the basis for the present analysis. This chapter connects their modelling assumptions, discretisation and verification, and examines their implications in the context of subsequent research.

Different numerical approaches address different aspects of variable-thickness shell dynamics. Dai, Cao and Chen [6] used a Haar wavelet discretisation for free vibrations of truncated conical shells with linear and parabolic thickness profiles. Their formulation is based on Love's first approximation and uses separation of variables to reduce the governing equations. This provides a useful methodological comparison with direct time integration in a shear-deformable model. However, a frequency calculation and a transient calculation answer different questions: the former characterises natural oscillations, whereas the latter also depends on the load history and initial conditions. A comparison between their numerical results requires compatible shell theories and boundary conditions.

Recent work has expanded the range of dynamic quantities and structural features considered. Hao, Sun, Zhang and Li [7] examined active travelling-wave vibration control of a rotating porous aluminium conical shell under impact loading. Their model includes elastic edge restraints, piezoelectric micro fibre composites and electromechanical coupling; differential and integral quadrature are used in the numerical treatment. The study is relevant to the present topic because it explicitly addresses travelling-wave response under impact. Its rotating, actively controlled structure is nevertheless distinct from the passive elastic shells considered here, so its results provide research context rather than a direct verification case.

Zhao, Gao, Li and Afshari [8] considered a conical shell whose thickness and graphene-nanoplatelet content vary along the meridian. Their first-order shear-deformation formulation combines an analytical circumferential treatment with differential quadrature along the meridian. Particle swarm optimisation is then used to seek thickness and reinforcement profiles that

increase the fundamental frequency and reduce mass. This 2026 contribution demonstrates the continuing role of spatially varying properties in shell design. For the present chapter, it also motivates a distinction between frequency-based optimisation and assessment of a transient displacement or stress maximum: improvement in one objective cannot be assumed to establish improvement in the other.

The recent study of three-layer hemispherical shells by Gaidaichuk, Kotenko and Mamedov [3] adds a complementary example involving structural inhomogeneity and nonstationary loading. Taken together, these contributions cover free vibration, transient motion, active control and optimisation, with different geometries and constitutive assumptions. Their relevance should therefore be assessed through the particular modelling choices they illuminate. The discussion below concentrates on variable-thickness conical shells and on the mathematical steps needed to connect their governing equations to the reported numerical response.

A central distinction is between an axisymmetric shell problem and a nonaxisymmetric shell or panel problem. In an axisymmetric reduction, compatible geometry, material properties, loading, initial data and restraints allow circumferential dependence to be eliminated. Meridional displacement, normal displacement and rotation then form the reduced system considered in detail here. Panels and nonaxisymmetric disturbances require additional displacement and rotation components together with circumferential derivatives. The axisymmetric derivation provides a starting point for understanding the method, but the additional variables and edge conditions of the two-dimensional problem must be accounted for when interpreting the panel examples [1].

The numerical approach adopted from the source material combines an integro-interpolation construction of spatial finite differences with explicit central differences in time [1]. Its mathematical interest lies in the treatment of variable coefficients and in the relation between balance equations, interface resultants and nodal motion. An explicit update also requires a stability restriction. The applicable time step must be connected to the spectrum of the actual discrete operator, including its boundary treatment; a bound on the magnitude of eigenvalues alone does not establish stability for an arbitrary nonsymmetric discretisation. This issue is considered alongside spatial refinement and the specification of initial data.

Verification and physical interpretation have separate roles. A comparison with an analytical solution and a mesh-refinement study test a calculation under specified conditions. Comparisons between thickness distributions then address a physical question within the verified scope. For each numerical example, the geometry, material data, load, restraints, observation position and normalisation must be stated or traced to the source. Similarly, the term wave process refers here to the evolution of disturbance fields resolved by the shell model. A time history at one point does not independently determine a propagation speed or identify a reflected wave; those conclusions require additional spatial and temporal evidence.

The purpose of this chapter is to connect the mathematical formulation, finite-difference approximation and interpretation of transient processes in elastic conical shells of variable thickness. Its contribution is a critical synthesis of the published formulation and numerical evidence, supported by an updated comparison with related numerical approaches. The treatment establishes the scope of the reduced and general problems and relates the verification results to the physical comparisons. The chapter proceeds through the governing model, numerical algorithm and selected examples to a discussion of their implications and applicability.

1. Mathematical Formulation

1.1 Geometry and Modelling Assumptions

We consider a truncated conical shell of variable thickness within a physically and geometrically linear shear-deformable theory [1]. Sections 1.1–1.6 give the axisymmetric meridional – normal formulation. Section 1.7 identifies the additional fields and edge conditions required for the nonaxisymmetric panel examples. The material is elastic, strains and rotations are small, and damping is omitted.

Let x be arc length along the generator measured from the smaller circular edge, and let θ be the cone semi-angle measured between the generator and the axis. The meridional length is L and the radius of the smaller edge is R_0. The circumferential coordinate is the azimuthal angle. The radius, surface measure and circumferential curvature are

$$r(x) = R_0 + x\sin\theta,\ 0 \le x \le L \tag{1}$$

$$dS = r(x)\,dx\,d\varphi,\ k(x) = \frac{\cos\theta}{r(x)} \tag{2}$$

The meridional curvature is zero. We assume $R_0 > 0$ so that the apex singularity is excluded. Positive normal displacement is directed outwards, consistently with the positive curvature term used below. The thickness is positive over the entire interval. For a linear profile, the end values h_a and h_β specify

$$h(x) = h_a + (h_b - h_a)\frac{x}{L}, h_a > 0, h_b > 0 \tag{3}$$

The coordinate origin is the smaller circular edge. The thickness profile must use this same origin. Material properties are independent of position unless stated otherwise; thickness variation alone changes geometry, stiffness and inertia.

A Winkler foundation may be retained as an optional normal restraint. Its coefficient $K \geq 0$ relates local restoring pressure to normal displacement. Setting $K = 0$ recovers the shell without an elastic foundation. No shear interaction within the foundation is included in this model.

1.2 Displacement Variables and Strain Measures

The unknown fields are the meridional displacement u(x,t), the outward normal displacement w(x,t), and the rotation β(x,t) of the normal in the meridional plane. They correspond to u_1, u_3 and φ_1 in the source formulation [1]. A prime denotes differentiation with respect to x and a superposed dot denotes differentiation with respect to time. Introduce the geometric coefficient

$$a(x) = \frac{r'(x)}{r(x)} = \frac{\sin\theta}{r(x)} \tag{4}$$

Within the adopted linear shear-deformation approximation, the meridional and circumferential membrane strains are

$$\varepsilon_s = u', \varepsilon_\theta = a u + k w \tag{5}$$

The transverse shear strain and changes of curvature are

$$\gamma = \beta + w', \chi_s = \beta', \chi_\theta = a\beta \tag{6}$$

Here γ is the engineering shear strain associated with the transverse shear resultant. The sign of β is fixed by the first relation in (6); an alternative rotation convention requires consistent changes in all subsequent equations. The relation $\varepsilon_\vartheta = a\,u + k\,w$ expresses two contributions to circumferential

extension: motion along the expanding cone and displacement in the normal direction.

The strain relations are the axisymmetric specialisation used in the selected source material. They should not be combined with a different shell kinematic theory without rederiving the force balances. In particular, retaining an independent rotation permits transverse shear deformation; it does not impose the zero-shear constraint $\beta = -w'$.

For subsequent use, N_s and N_ϑ denote meridional and circumferential membrane resultants, Q denotes the transverse shear resultant, and M_s and M_ϑ denote the corresponding bending moments. Their units are force per unit length for N_s, N_ϑ and Q, and moment per unit length for M_s and M_ϑ. The quantities ε_s, ε_ϑ and γ are dimensionless, whereas χ_s and χ_ϑ have units of inverse length.

1.3 Constitutive Relations and Variable Stiffness

For a homogeneous orthotropic material whose principal axes follow the meridian and circumference, use a symmetric reduced elastic matrix. This notation makes reciprocity explicit and avoids interchanging Poisson-ratio indices. Let E_s and $E\vartheta$ be the principal Young moduli, $\nu_s\vartheta$ the circumferential contraction ratio under meridional uniaxial stress, and $\nu\vartheta_s$ the reciprocal ratio. We assume positive Young moduli, positive effective shear modulus and positive mass density; together with $\Delta > 0$ these ensure a positive-definite constitutive law and positive inertia coefficients in the reduced model.

$$\frac{\nu_{s\theta}}{E_s} = \frac{\nu_{\theta s}}{E_\theta},\ \Delta = 1 - \nu_{s\theta}\nu_{\theta s} > 0 \tag{7}$$

$$C_{11} = \frac{E_s}{\Delta}, C_{22} = \frac{E_\theta}{\Delta}, C_{12} = \frac{\nu_{\theta s}E_s}{\Delta} = \frac{\nu_{s\theta}E_\theta}{\Delta} \tag{8}$$

The membrane and bending coefficients at each position are

$$A_{ij}(x) = h(x)C_{ij}, D_{ij}(x) = \frac{h^3(x)}{12}C_{ij} \tag{9}$$

$$N_s = A_{11}\varepsilon_s + A_{12}\varepsilon_\theta, N_\theta = A_{12}\varepsilon_s + A_{22}\varepsilon_\theta \tag{10}$$

$$M_s = D_{11}\chi_s + D_{12}\chi_\theta, M_\theta = D_{12}\chi_s + D_{22}\chi_\theta \tag{11}$$

$$Q = S(x)\gamma,\ S(x) = G^* h(x) \tag{12}$$

G* is the effective transverse shear modulus in the adopted resultant law. It corresponds to the coefficient multiplying thickness in the source shear stiffness. If a shear correction factor is used, it is absorbed into G* and must be specified in the numerical example. No additional factor is assumed here.

For an isotropic material, $E_s = E_\vartheta = E$ and $\nu_{s\vartheta} = \nu_{\vartheta s} = \nu$. The membrane coefficients scale with h and the bending coefficients with h^3. Consequently, equal-mass shells can have different local bending stiffness distributions. The inertia coefficients are $m(x) = \rho h(x)$ and $J(x) = \rho h^3(x)/12$, where ρ is the mass density. The model assumes a material distribution symmetric about the reference midsurface, so membrane–bending coupling is absent.

1.4 Variational Statement and Equations of Motion

Let p(x,t) be an outward normal load per unit midsurface area. For the present axisymmetric system, introduce the potential energy U, kinetic energy T and virtual work δW. With integrations over $0 \le x \le L$, they are

$$U = \pi \int_0^L r\left[N_s \varepsilon_s + N_\theta \varepsilon_\theta + Q\gamma + M_s \chi_s + M_\theta \chi_\theta + Kw^2 \right] dx \tag{13}$$

$$T = \pi \int_0^L r\left[m\left(u^{\cdot 2} + w^{\cdot 2}\right) + J\beta^{\cdot 2} \right] dx \tag{14}$$

$$\delta W = 2\pi \int_0^L rp\,\delta w\,dx, \int_{t0}^{t1} \left(\delta U - \delta T - \delta W\right) dt = 0 \tag{15}$$

Variations vanish at the initial and final times. Substitution of (5)–(12), followed by integration by parts in space and time, gives the following balance equations. Their signs are consistent with outward positive w and $\gamma = \beta + w'$:

$$\frac{1}{r}\left(rN_s\right)' - aN_\theta = mu \tag{16}$$

$$\frac{1}{r}\left(rQ\right)' - kN_\theta - Kw + p = m\,w \tag{17}$$

$$\frac{1}{r}\left(rM_s\right)' - aM_\theta - Q = J\beta \tag{18}$$

The geometric terms aN_ϑ and aM_ϑ arise from ε_ϑ and χ_ϑ. They do not differentiate the circumferential resultants with respect to x. In contrast, the meridional resultants appear inside the derivatives of rN_s and rM_s. This distinction is essential when constructing the difference equations.

Equations (16)–(18) follow from the stated energy and strain relations. The variable stiffness coefficients remain inside the differentiated resultants;

replacing them by spatially uniform coefficients would define a different model.

1.5 Boundary Conditions and Initial State

Spatial integration by parts produces the boundary virtual work

$$2\pi[r(N_s\delta u+Q\delta w+M_s\delta\beta)]_0^L \quad (19)$$

Thus, at either circular edge, each displacement variable is paired with its corresponding resultant. The edge conditions must be selected to represent the physical support. A completely clamped edge imposes

$$u=0,\ w=0,\ \beta=0 \quad (20)$$

At a free edge with no applied line force or line moment, the natural conditions are

$$N_s=0,\ Q=0, M_s=0 \quad (21)$$

A free circular edge carries no meridional membrane force, transverse shear force or meridional bending moment. Nonzero edge actions must use signs consistent with the outward edge conormal. The two circular edges may have different support types.

For a shell initially at rest and without an initial deformation, the initial conditions are

$$u(x,0)=w(x,0)=\beta(x,0)=0 \quad (22)$$

$$\dot{u}(x,0)=\dot{w}(x,0)=\dot{\beta}(x,0)=0 \quad (23)$$

The reduced system contains three unknown fields, so only their three initial displacements and three initial velocities are prescribed. A circumferential displacement is not introduced into these initial conditions because it is absent from the axisymmetric meridional–normal model.

A distributed pulse is represented by its actual spatial and temporal dependence p(x,t). Its amplitude, duration and shape must be stated for every numerical example. A spatially uniform pressure pulse is compatible with axisymmetry, but axisymmetry does not require the pressure to be uniform along the meridian. The load must also be distinguished from the foundation reaction −Kw.

1.6 Consistency Checks and Scope of the Formulation

The variational formulation supplies a useful energy identity. For stationary supports, no applied edge actions and a time-independent elastic foundation, equations (16)–(18) imply

$$\frac{d}{dt}\left(T+U\right)=2\pi\int_0^L rp\,\dot{w}\,dx \tag{24}$$

After the external pulse has ended, the continuous undamped model conserves total mechanical energy. This identity is a consistency property of the equations. It is not a claim that the discrete algorithm conserves energy exactly; its discrete behaviour must be examined separately.

Several limiting cases help check an implementation. Setting $h_a = h_\beta$ removes thickness variation, and setting K = 0 removes the foundation. In the cylindrical limit θ = 0, r becomes constant, a vanishes and $k = 1/R_0$. The curvature coupling between normal motion and hoop extension remains. These reductions can be checked before computing a variable-thickness cone.

The mathematical model describes reversible elastic motion within the selected linear shell approximation. It does not include plasticity, damage, large rotations, material damping or a three-dimensional description of thickness-direction wave propagation. The wave-related interpretation of its solutions therefore concerns the displacement and resultant fields resolved on the shell midsurface.

The reduced formulation uses a common coordinate origin, reciprocal orthotropic coefficients and boundary resultants consistent with the energy variation. These conventions must also be used in the discrete equations and in interpreting the reported numerical examples [1].

1.7 Nonaxisymmetric Shells and Panels

For a panel, the midsurface domain is $0 \le x \le L$, $0 \le \varphi \le \varphi_0$, where φ is the azimuthal angle and φ_0 is the opening angle. The five generalised displacement fields in the source model are the meridional, circumferential and normal displacements u, v and w, and the independent rotations β_s and βφ [1]. Each depends on x, φ and time. The source notation for these fields is u_1, u_2, u_3, φ_1 and φ_2. Thus β_s reduces to β in the meridional–normal problem.

The general energy includes circumferential derivatives, in-plane shear and twisting terms, and a second transverse shear contribution. Its kinetic energy includes the translational terms for all three displacements and rotary inertia for both rotations. Consequently, the circumferential displacement

and rotation cannot be introduced as passive extra coordinates: their strain measures, constitutive coefficients and balance equations are required. Equations (5)–(12) state only the reduced relations; the full component formulation remains that of the source monograph [1].

At a clamped panel edge, all five displacement and rotation fields vanish. At an unloaded free edge, the five generalised edge actions conjugate to those fields vanish: two in-plane line forces, one transverse line force and two line moments. These actions follow from the boundary term of the full virtual-work statement and depend on whether the edge is circular or follows a generator. The three conditions in (21) describe only the axisymmetric circular-edge reduction and must not be applied unchanged to every panel edge.

Initial displacement and velocity fields are specified for all five unknowns and must satisfy the prescribed kinematic edge conditions. A closed shell instead requires periodic displacement and rotation fields around its circumference, together with the corresponding continuity of internal actions. The meridional–normal reduction requires circumferentially independent data and $v = \beta\varphi = 0$; axisymmetry alone does not exclude a separate torsional motion. A panel with restrained generator edges generally does not admit that reduction, even under spatially uniform normal pressure.

This distinction defines how the subsequent examples are used. The detailed derivation in Sections 1.1–1.6 supports the axisymmetric calculation, whereas the nonaxisymmetric panel results refer to the full source model [1]. A new computation of those panel cases requires its complete component equations, material shear coefficients and discrete edge closures. Agreement in an axisymmetric benchmark alone cannot verify those additional parts of the implementation.

2. Numerical Algorithm

2.1 Spatial Difference Scheme

The source method combines an integro-interpolation spatial approximation with explicit central differences in time [1]. Equation (25) displays the meridional balance in a midpoint form on a uniform mesh. The interface resultants retain the local thickness and elastic coefficients. Cell integration, coefficient quadrature and boundary closure are parts of the spatial discretisation and must be specified consistently; the displayed

interior equation alone does not establish the accuracy or stability of the complete method.

Let the meridional mesh contain N intervals of length $\Delta x = L/N$, with nodes $x_i = i\Delta x$. The interface between nodes i and i+1 is at $x = (i+1/2)\,\Delta x$. Displacements and rotation are stored at integer nodes and time levels $t^n = n\Delta t$. Interface strains use centred differences and averages of the adjacent displacement values; the constitutive relations are evaluated at the same interface. A circumferential resultant appearing as a nodal source term requires a consistent interpolation from the neighbouring interfaces.

$$\frac{1}{r_i}\frac{\left(rN_s\right)^n_{i+1/2}-\left(rN_s\right)^n_{i-1/2}}{\Delta x}-a_i N\theta_i^n = m_i\frac{u_i^{\,n+1}-2u_i^{\,n}+u_i^{\,n-1}}{\Delta t^2} \tag{25}$$

Equation (25) is the difference analogue of the meridional balance equation (16); the normal and rotational balance equations (17)–(18) are discretised in the same way, each resultant being evaluated at the half-integer node from the strain and curvature measures (5)–(6) formed from the current displacement field. Collecting the three discrete equations at all interior nodes gives, in matrix-vector form,

$$M\,\tilde{q}+K\,\bar{q}=F\left(t\right) \tag{26}$$

Here $\bar{q}$ contains the unconstrained nodal displacement and rotation variables after prescribed kinematic conditions have been eliminated. M is the positive diagonal mass matrix of the chosen lumped discretisation; K is its stiffness operator and $\bar{F}$ contains the external loading and prescribed-boundary contributions. K must not be confused with the scalar Winkler coefficient in Section 1. Its symmetry depends on the spatial construction, weighting and edge closure. Positivity of the continuous elastic energy alone does not establish the required properties of an independently assembled discrete operator. With these definitions, the explicit update is

$$q^{-n+1}=2q^{-n}-q^{-n-1}+\Delta t^2 M^{-1}\left(F^n-K\bar{q}^n\right) \tag{27}$$

The update uses two successive displacement states and a local stiffness action, avoiding a linear solve at every time step. Its initialisation must include the prescribed initial velocity. Let $\bar{V}^0$ denote that velocity and $a^{-o}=M^{-1}\left(F^o-Kq^{-o}\right)$ the initial acceleration. A second-order start is $q^{-1}=q^{-o}+\Delta t V^o+\left(\Delta t^2/2\right)a^{-o}$. Setting $\bar{q}^1$ equal to $\bar{q}^0$ would generally lose this consistency when the initial velocity or load is nonzero.

2.2 Stability of the Explicit Scheme

For the undamped homogeneous problem, define A = $M^{-1}K$. First assume that A is diagonalisable with real positive eigenvalues. This holds, for example, when M is symmetric positive definite and K is symmetric positive definite, because A is then similar to a symmetric positive-definite matrix. In each mode the central-difference recurrence has characteristic equation $z^2-\left(2-\Delta t^2\lambda\right)z+1=0$. Its roots are distinct and lie on the unit circle when $0<\Delta t^2\lambda<4$. Consequently, a strict time-step restriction for the positive-frequency modes is

$$\Delta t<\frac{2}{\omega_{\max}},\ \omega_{\max}{}^2=\lambda_{\max}\left(M^{-1}K\right) \tag{28}$$

The endpoint $\Delta t\omega_{max}$ = 2 is excluded: the highest-frequency recurrence then has a repeated root z = −1 and admits a linearly growing component. If free supports introduce zero-frequency rigid-body modes, these must be identified separately; their linear-in-time displacement under an initial rigid-body velocity is physical. Complex eigenvalues, negative eigenvalues or defective eigenvectors invalidate the preceding modal argument. For a nonsymmetric spatial operator, its spectral properties or an appropriate discrete energy estimate must therefore be established before (28) is used.

A computable conservative bound is obtained from the absolute row sums: $B=max_i\sum_j\left|A_{ij}\right|$, giving |λ| ≤ B. Under the stated modal assumptions and B > 0, choose $\Delta t=2\eta/\sqrt{B}$ with 0 < η < 1. The row sums must include the actual edge closure and foundation contribution. When translations and rotations use different units, first scale the unknowns consistently; apply the estimate to the resulting similar operator. This changes the conservatism of the bound but not its eigenvalues. The bound limits eigenvalue magnitudes; it does not itself prove that they are real, positive or associated with a complete modal basis.

2.3 Extension to the Two-Dimensional Problem

Nonaxisymmetric motion requires the five-field shell formulation described in Section 1.7. Its component equations and constitutive relations are taken from the general source model [1]. They include in-plane shear, twisting and circumferential transverse shear in addition to the quantities

in (5)–(12); the three-field axisymmetric equations alone do not define this problem.

The source applies the integro-interpolation principle on a two-dimensional meridional–circumferential mesh [1]. The explicit central-difference time update then advances all five fields. Circular and generator edges require their own five-component boundary treatment, as described in Section 1.7. For a closed shell, circumferential periodicity replaces the generator-edge conditions. The full two-dimensional stencil is not reproduced here; the panel examples are discussed as results of the source implementation.

In two dimensions the stability analysis must use the combined discrete operator, including both spatial directions and their coupling terms. Taking the smaller of two independently derived one-dimensional time-step limits is not generally sufficient. Circumferential angular spacing must also be interpreted through the local physical length $r(x)\Delta\varphi$. A row-sum estimate may be evaluated from the full local stencil without storing a dense matrix. Verification of the axisymmetric limit is useful, but it does not replace tests of the circumferential terms and panel-edge closures.

2.4 Computational Remarks

For a fixed local stencil, evaluating interface resultants and nodal residuals requires storage proportional to the number of degrees of freedom. This is $O(N)$ for the meridional mesh and $O(N_x N\varphi)$ for a two-dimensional mesh. Matrix-free evaluation is a property of this local implementation; explicit time integration alone does not guarantee a sparse or local spatial operator.

Each time step comprises evaluation of strains and resultants, formation of the residual forces and moments, and the update (27). Prescribed displacements are enforced consistently at the required time levels. A free edge instead requires a discrete natural-boundary closure; it cannot be implemented merely by resetting displacement values after the update. Changes in edge restraint require reevaluation of the stability bound.

Spatial and temporal errors should be examined separately. Refining the mesh changes both the approximation error and the admissible time step; reducing Δt below its stability limit is still necessary when the load

duration or response phase demands greater temporal resolution. With a uniform global time step, local mesh refinement can tighten the step limit, although reducing the total number of nodes relative to a uniformly fine mesh may still save work. The fixed-mesh modal argument above is not a proof of convergence for an entire mesh family: that additionally requires consistency, controlled boundary errors and uniform stability estimates. The published verification cases in Section 3 supply evidence only for the configurations actually tested.

3. Verification and Numerical Examples

This section analyses the verification tests and numerical examples reported in [1]. It distinguishes meridional mesh refinement, comparison with an analytical solution, time-step sensitivity in the nonaxisymmetric problem, and comparisons between physical configurations. The reproduced values and curves are evaluated within the stated test conditions, with numerical accuracy assessed separately from differences between shell configurations.

3.1 Convergence with Mesh Refinement

The source mesh-refinement test concerns a constant-thickness cone with clamped circular edges under a spatially uniform half-sine pressure pulse. Its meridional length is 0.8 m, thickness 0.02 m, smaller-edge radius 0.2 m and cone semi-angle $\pi/12$. The pulse amplitude is 10^6 Pa and its duration is 0.625L/c, where c is the extensional speed defined below. Maximum normal displacement and circumferential normal stress are examined at the meridional midpoint during the first oscillation period. The loading and material-speed definition follow [1].

Explicitly, the pressure during the pulse is $p(t)=p\cdot sin\left(\frac{\pi t}{T}\right), 0\le t\le T$, and it vanishes outside this interval. The extensional speed satisfies $c^2=\frac{E}{\rho\left(1-\nu^2\right)}$. Here p_0 is the pressure amplitude, and T denotes pulse duration, distinct from the kinetic energy in Section 1.4.

Table 1

Maximum normal displacement and circumferential stress at the meridional midpoint under meridional mesh refinement.

Mesh parameter N	Maximum w (10^{-4} m)	Maximum σ_{22} (10^{8} Pa)
20	0.850	0.142
40	0.879	0.146
80	0.885	0.147
160	0.886	0.147
320	0.886	0.147

The two finest rows coincide at the displayed precision. The source selects N = 160 as adequate for this test. The printed displacement change between N = 80 and N = 160 is approximately 0.11% relative to the latter value; identical rounded stress entries do not demonstrate zero error. The column units retain the source scales, rather than describing the values as dimensionless normalised quantities.

3.2 Comparison with an Analytical Solution

The numerical and analytical displacement distributions are compared for a constant-thickness cone with clamped circular edges [1]. Young's modulus is 2.1×10^{11} Pa, Poisson ratio is 0.3 and density is 7.8×10^{3} kg/m³; the geometry is that stated in Section 3.1. The spatial deflection profiles show satisfactory agreement. This comparison provides a qualitative benchmark; a quantitative error estimate would require an error norm evaluated from the underlying numerical and analytical data.

3.3 Axisymmetric Example: Shell on an Elastic Foundation

The axisymmetric foundation example concerns a cone with clamped circular edges, length 0.4 m and smaller-edge radius 0.3 m, with thickness increasing from 0.005 m to 0.010 m [1]. The prescribed Winkler coefficient is 2.5×10^{7} N/m³ and the loading is a spatially uniform half-sine normal pressure pulse. The calculations cover 200 pulse durations. At this fixed coefficient, the foundation influence becomes apparent from approximately 100 pulse durations onward. This time dependence characterises the evolution of the supported and unsupported solutions.

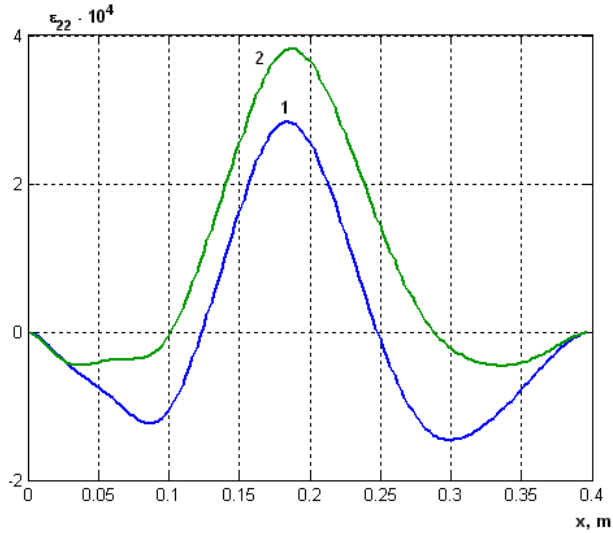


Figure 1. Circumferential strain along the meridian at 197 pulse durations and cone semi-angle π/6: curve 1, shell on the Winkler foundation; curve 2, shell without the foundation.

Figure 1 shows a lower positive strain peak for the shell on the foundation in this particular comparison. The curves also differ in the negative-strain regions. This illustrates a redistribution of the strain field at the selected instant, rather than a uniform scaling of the entire response. It does not establish that the foundation reduces every response component or every peak over the complete time interval.

Phase differences can accumulate during an undamped transient calculation, making the observation interval essential to interpretation. Figure 1 compares the two configurations at the same instant; the equal-mass panel comparison below instead uses instants associated with their respective displacement maxima. For the foundation example, [1] reports Young's modulus as 7×10^{11} Pa and Poisson ratio as 0.3. These reported material data are retained for the interpretation of Figure 1.

3.4 Nonaxisymmetric Time-Step Verification and the Clamped–Free Panel

The nonaxisymmetric verification examines meridional and circumferential strain histories at cone semi-angle $\pi/4$ [1]. Figure 2 shows these two components: curve 1 is the meridional strain and curve 2 is the circumferential strain. The temporal refinement study varies the time step from 10^{-6} to 10^{-9} s and compares strain values at 1.25×10^{-4} s and 2.15×10^{-4} s.

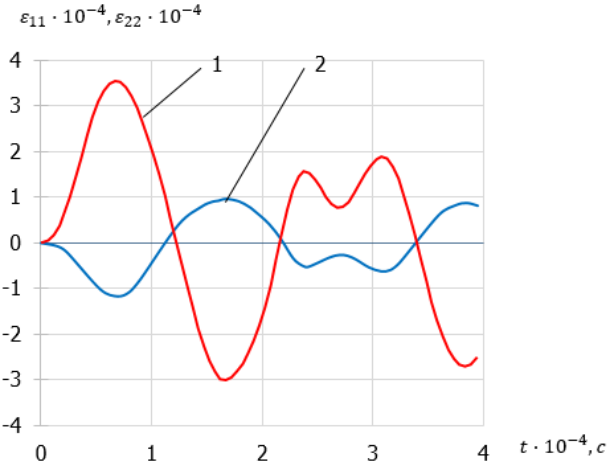


Figure 2. Meridional strain (curve 1) and circumferential strain (curve 2) versus time at cone semi-angle $\pi/4$. The plotted time coordinate is in units of 10^{-4} s.

The source regards a time step of 10^{-8} s as adequate for the reported test. However, its tabulated values do not become identical at all subsequent refinements. For example, two strain entries change from 0.3202 to 0.3262 and from 0.03121 to 0.03253 when the step decreases from 10^{-8} to 10^{-9} s. These comparisons correspond to approximately 1.8% and 4.1% relative differences, respectively, using the finer-step value as denominator. The ratios are calculated from the printed table; they are not errors measured against an exact solution.

The later clamped–free panel example in the source has three clamped edges and one free edge. Its response varies with cone semi-angle and with

the time at which each field reaches its maximum magnitude [1]. Those physical comparisons should be distinguished from the time-step test above. In particular, Figure 2 alone does not demonstrate circumferential mesh convergence or convergence specifically at the free edge.

3.5 Nonaxisymmetric Example: Fully Clamped Panel of Equal Mass

The fully clamped panel example compares variable thickness with constant thickness at equal mass [1]. The panel has meridional length 0.4 m, smaller-edge radius 0.3 m and angular extent $\pi/3$, centred on the source coordinate $s_2 = 0$. Its thickness increases from 0.005 m to 0.015 m. Young's modulus is 7×10^{10} Pa and Poisson ratio is 0.3. The comparison shown here uses cone semi-angle $\pi/12$. Both panels are initially at rest and undergo the same half-sine normal pressure pulse. The reported modulus-to-pressure-amplitude ratio is 7×10^4, corresponding to a pressure amplitude of 10^6 Pa. The pulse duration is 0.625L/c, with c defined in Section 3.1.

The source reports a difference of the order of 25% between the maximum displacement magnitudes [1]. The profiles in Figure 3 are taken at different instants: 16.7 pulse durations for the variable-thickness panel and 13.1 pulse durations for the constant-thickness panel. This is a configuration-specific comparison of displacement maxima, not a common percentage change for displacement, strain and stress. The source does not explicitly state the denominator used for its approximate percentage.

Figure 3 also shows that the extrema need not occur at exactly the same meridional coordinate. Equal mass controls the total material quantity, but does not preserve the distributions of membrane stiffness, bending stiffness or inertia. The observed difference therefore concerns the combined effect of those distributions under the stated loading and restraints. It should not be interpreted as a universal reduction achievable by any thickness variation.

Figure 4 shows that thickness redistribution changes both the sign and spatial location of strain extrema. The variable-thickness panel exhibits a more pronounced negative extremum in the first part of the meridian, whereas the constant-thickness panel has a larger positive extremum in the second part. The displacement comparison and the strain profiles therefore characterise different aspects of the deformation field; the approximate displacement difference cannot be transferred directly to the strain extrema.

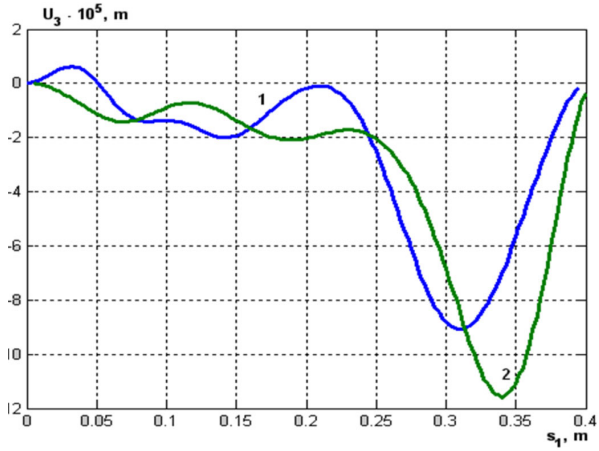


Figure 3. Normal displacement along the central meridian: variable thickness (curve 1, time 16.7T) and equal-mass constant thickness (curve 2, time 13.1T), where T is pulse duration

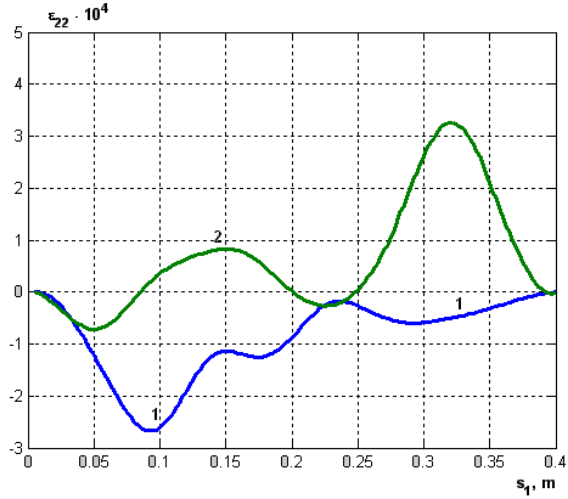


Figure 4. Circumferential strain along the central meridian for the variable-thickness panel (curve 1) and equal-mass constant-thickness panel (curve 2)

The selected examples demonstrate the importance of identifying response components, locations and observation times. Foundation effects evaluated at a common instant describe the evolving difference between two solutions. Displacement maxima selected at different instants instead compare the peak response attained by each configuration over the examined interval. Together with the strain profiles, these observations support a component-specific assessment of thickness redistribution.

3.6 Summary of the Numerical Examples

Table 2 identifies the source evidence associated with each example. It separates numerical verification from physical comparisons and records the limits of the conclusions supported by the reproduced material.

Table 2

Scope of the verification tests and physical comparisons in [1]

Example (§)	Geometry / support	Loading	Principal finding
3.1	Constant-thickness cone, clamped edges	Impulsive, uniform	Midpoint maxima stabilise at the printed precision between N = 160 and N = 320
3.2	Constant-thickness cone, clamped edges	Impulsive, uniform	Numerical and analytical spatial deflection profiles agree satisfactorily in the source comparison
3.3	Variable-thickness cone, clamped, Winkler foundation	Impulsive, uniform	At fixed foundation stiffness, an effect is reported from about 100 pulse durations onward
3.4	Nonaxisymmetric strain test; separate clamped–free panel example	Distributed impulsive	Source time-step comparison is separate from the cone-angle study of the clamped–free panel
3.5	Variable- vs. equal-mass constant-thickness panel, all edges clamped	Distributed impulsive	About 25% difference is reported for displacement maxima; strain profiles require separate interpretation

Table 2 shows that verification is quantity- and configuration-dependent. Stabilisation of the axisymmetric midpoint values does not imply that every panel strain is mesh-independent. Likewise, a physical difference between

two thickness profiles must not be labelled numerically exact without a corresponding convergence assessment. The examples support the stated comparisons within the published evidence; their extension to other geometries, restraints or response measures requires additional calculations.

4. Discussion

4.1 Interpretation of the Published Numerical Evidence

The examples in Section 3 address different questions and should be read as complementary pieces of evidence. The constant-thickness benchmark compares spatial displacement profiles with an analytical solution. Table 1 examines the meridional mesh dependence of selected response maxima. The nonaxisymmetric test examines sensitivity to the time increment, while the foundation and equal-mass examples illustrate changes in the physical response. Agreement in one of these tests cannot substitute for the others: a stable calculation may retain appreciable phase error, and a converged displacement does not establish convergence of every stress component.

The distinction matters for the interpretation of the source mesh study. Its reported normal displacement changes by approximately 0.11% between N = 80 and N = 160, and the last two values coincide at the printed precision. This is useful evidence of stabilisation of that observable. It neither determines a convergence order nor establishes an exact error bound. Similarly, the selected values in the nonaxisymmetric time-step study retain differences of approximately 1.8% and 4.1% between the two smallest increments for particular components and observation instants. These differences are comparisons between tabulated numerical values, not errors relative to an exact solution.

Thickness redistribution changes several terms of the governing equations simultaneously. For a homogeneous material, membrane stiffness and translational inertia scale with h, whereas bending stiffness and rotary inertia scale with h cubed. A thickness increase therefore changes local resistance to bending and the coupling between translational and rotational motion, as well as mass. The response of a finite cone also depends on curvature, loading and reflection at its boundaries. The resulting maxima cannot generally be predicted from the thickness ratio alone or represented by a single correction to a constant-thickness solution.

In the fully clamped equal-mass panel example, the reported displacement difference of the order of 25% concerns maxima reached at different instants. The comparison therefore combines changes in response amplitude, spatial distribution and timing. The source does not specify the denominator of that percentage, so it should be retained as an approximate reported comparison rather than converted into a precise reduction factor. The accompanying circumferential strain profiles have different signs and locations of extrema. They provide additional information about redistribution of deformation but do not establish the same percentage change in strain or stress.

The foundation example has a different interpretation. At the fixed foundation stiffness considered in the source, the supported and unsupported responses become observably different at later times, reported as $t \geq 100T$. This is a statement about the observation interval, not a threshold value of foundation stiffness. An elastic foundation stores and returns energy; the Winkler term used here introduces no dissipation. Consequently, changes in a selected strain peak may reflect altered modal frequencies and phase relationships, and should not be described as damping or uniform suppression of the transient response.

4.2 Relation to Recent Shell Dynamics Research

Recent studies extend conical-shell dynamics through different representations of structural inhomogeneity. Gaidaichuk, Kotenko and Mamedov [9] analyse three-layer conical shells with polymer filling and discrete reinforcement using shear-deformable shell and rod descriptions with finite-element modelling. They examine how bearing-layer and filler properties affect deflections and normal stresses. This work is relevant to the present treatment because it also relates spatially distributed stiffness to transient response. Its layered construction and discrete reinforcement, however, require additional mechanical descriptions; its numerical results are not a benchmark for the single-layer model used here. The hemispherical study [3] provides a further geometrically distinct comparison.

The active travelling-wave control study [7] and the frequency and mass optimisation study [8] address two further directions. The former includes smart composite actuation and feedback in an elastically supported conical shell, whereas the latter combines variable thickness with graded reinforcement and an optimisation procedure. Their objectives differ from

interpreting a prescribed pulse response in a passive homogeneous shell. For the present chapter, they motivate separating the choice of thickness distribution from the criterion used to judge it. A profile selected for an eigenfrequency or mass objective need not minimise the largest displacement during a specified transient event.

Khalmuradov, Khudoynazarov and Ismoilov [10] formulate torsional vibrations of a truncated conical shell interacting with an elastic medium and examine a harmonic torsional-wave example through a frequency–wavenumber relation. This highlights a separate branch of motion. Independence of the circumferential coordinate does not, by itself, eliminate torsion: the three-field formulation in Section 1 additionally restricts motion to the meridional and normal components and the associated rotation. It therefore cannot describe the torsional problem of [10]. Likewise, response histories at one observation point in the present examples do not determine a dispersion relation or uniquely identify wave propagation speeds.

These comparisons locate the chapter within current research without treating unlike models as interchangeable. Direct numerical validation would require matching geometry, constitutive properties, loading, boundary conditions and response definitions. A finite-element result may serve as an independent numerical comparison when those conditions are met, but the use of a different discretisation alone does not make it an exact reference. The strongest assessment combines analytical limiting cases, independent implementations and systematic refinement for the quantities actually used in interpretation.

5. Practical Implications for Modelling and Design

5.1 Defining the Response Criterion

An equal-mass comparison should preserve the same midsurface geometry, material, support conditions and loading while changing the thickness distribution. The reference constant thickness must be obtained from the surface-area-weighted mass integral; for a cone, an unweighted average along the meridian is generally insufficient. Each result should identify whether it represents a value at a prescribed point and time, a spatial maximum at a selected instant, or a maximum over the entire observation interval. These definitions answer different design questions and should be fixed before profiles are ranked.

A displacement criterion alone does not characterise the full stress–strain state. The location of the largest strain may shift as thickness varies, and tensile and compressive extrema may respond differently. Design-oriented interpretation should therefore retain the relevant displacement, strain and stress measures separately, together with their positions and times. No strength, buckling or fatigue assessment is established by the response comparisons in this chapter; those assessments would require their own material data, governing criteria and, where appropriate, additional physical modelling.

5.2 Choosing the Mesh, time Increment and Observation Interval

Spatial resolution and temporal accuracy require separate checks even though their admissible choices are coupled. Refining the spatial mesh changes the discrete operator and can increase its highest frequency, reducing the stable time increment. For the central-difference scheme, the restriction in Section 2 applies to the complete constrained operator, including meridional and circumferential coupling and the implemented boundary treatment. A local stiffness-to-inertia estimate can guide an initial choice, but it does not replace that operator-level check.

Once a stable increment has been selected, it should be reduced further to examine temporal accuracy at a fixed spatial mesh. Spatial refinement should then be assessed with a sufficiently small increment so that time-discretisation effects do not dominate the comparison. Peak values, their timing and representative field profiles are useful complementary observables. For stresses obtained from spatial derivatives, refinement should be evaluated directly rather than inferred from displacement convergence. The mesh and increment adequate for one pulse duration or boundary condition cannot be assumed adequate for another.

The observation interval is part of the problem definition. Conservation of total mechanical energy after the pulse does not imply constant displacement or strain at individual points. Energy continues to exchange between kinetic and elastic forms and between coupled motions, while modal superposition can generate later local maxima. The late foundation effect in Section 3 illustrates why an interval limited to the initial pulse can miss a relevant difference. A calculation intended to estimate the largest response should report its finite observation interval and check whether extending that interval changes the selected maximum.

5.3 Model Scope and Reproducibility

The linear shear-deformable description retains transverse shear and rotary inertia but excludes plasticity, damage, large rotations and material damping. It does not resolve a general three-dimensional wave field through the wall thickness. These assumptions should be assessed against the geometry and duration of the applied excitation. A sharply changing thickness, layered wall or different elastic support may require revised constitutive or interface relations and a new boundary treatment, as well as renewed numerical verification. Such changes cannot always be introduced merely by replacing coefficient values in an existing recursion.

The spatial discretisation and time integrator are also distinct choices. Finite differences and finite elements can both be combined with explicit or implicit time integration. The advantage of an explicit update depends on how the mass operator is represented or inverted; conditional stability then constrains the number of required steps. For a regular conical coordinate grid, the source finite-difference construction offers a direct treatment of variable coefficients. More complex geometry may favour a finite-element representation, but computational efficiency requires an actual comparison at matched accuracy rather than a general claim based on the method name.

Reproduction of the panel examples requires the full nonaxisymmetric component equations, spatial stencils and boundary closures given in the source formulation [1]. The reduced variational model developed here establishes the coupling of meridional and normal motion, while Sections 1.7 and 2.3 identify the additional fields needed for panels. Together, these formulations define the scope of the numerical examples and the verification requirements for extending the method to other geometries or restraints.

CONCLUSIONS

The chapter presents a mathematical and numerical interpretation of transient processes in elastic conical shells with variable meridional thickness, drawing on the published results of [1], [4] and [5]. The reduced variational formulation makes the coupling between geometry, membrane and bending stiffness, shear deformation and inertia explicit. Nonaxisymmetric panel examples require the additional displacement and rotation fields of the full source model. The analysis therefore distinguishes the equations developed

here in detail from the broader numerical configurations discussed through published evidence.

The explicit central-difference procedure has a conditional stability restriction governed by the complete discrete operator. A conservative absolute-row-sum estimate is useful only when the required spectral properties have been established. Stability and convergence are separate questions: the meridional mesh study and the analytical spatial-profile comparison support the tested source calculations, while the nonaxisymmetric time-step data show that selected components remain sensitive to further refinement. This evidence does not establish general convergence for all geometries, boundary closures or response measures.

Variable thickness changes the amplitude, position and timing of the transient response. In the fully clamped equal-mass panel example, the source reports a displacement-maximum difference of the order of 25% at separately selected peak-response instants. The accompanying strain distributions require independent interpretation and do not support applying that percentage to every strain or stress component. At the fixed stiffness used in the foundation example, the reported late-time divergence of supported and unsupported responses demonstrates the importance of the observation interval; it does not establish dissipative attenuation or a stiffness threshold.

The practical implication is that thickness distribution should be evaluated against a clearly defined response criterion, with spatial and temporal refinement appropriate to that criterion. Local extrema may continue to change after the load has ended even when total mechanical energy is conserved. Reports should therefore identify the observation interval, the locations and times of extrema, and the conditions used to compute them. A converged displacement history alone is insufficient evidence for the accuracy of derived stresses or for a structural strength assessment.

Recent research on layered shells, active wave control, graded-material optimisation and torsional motion places these results in a broader context. Those developments offer directions for further investigation while introducing mechanisms beyond the present passive single-layer model. The chapter contributes a mathematical synthesis and critical interpretation of the published evidence, connecting thickness-dependent stiffness and inertia with displacement and strain behaviour. Extensions to more complex

structures require the corresponding governing relations, a reproducible implementation and verification appropriate to the selected response measures.

References:

1. Luhovyi P. Z., Meish V. F., Meish Yu. A. (2022). Dynamika konstruktyvno-neodnoridnykh obolonkovykh struktur [Dynamics of structurally inhomogeneous shell structures]. Kyiv: Lira-K, 336 p. (in Ukrainian)

2. Lugovoi P. Z., Meish V. F. (2017). Dynamics of inhomogeneous shell systems under non-stationary loading (survey). *International Applied Mechanics*, vol. 53, pp. 481–537. DOI: https://doi.org/10.1007/s10778-017-0833-3

3. Gaidaichuk V., Kotenko K., Mamedov A. (2025). Dynamics of a three-layer hemispherical shell under non-stationary loading. *Strength of Materials and Theory of Structures,* no. 114, pp. 83–93. DOI: https://doi.org/10.32347/2410-2547.2025.114.83-93

4. Meish V. F., Meish Yu. A., Melnyk V. M. (2014). Chyselne modeliuvannia dynamichnoi povedinky konichnoi obolonky zminnoi tovshchyny pry dii rozpodilenoho impulsnoho navantazhennia [Numerical modelling of the dynamic behaviour of a conical shell of variable thickness under a distributed impulsive load]. *Problemy obchysliuvalnoi mekhaniky i mitsnosti konstruktsii*, no. 22, pp. 169–181. (in Ukrainian).

5. Meish V. F., Galagan O. G., Mel'nik V. M. (2014). Nonaxisymmetric vibrations of conical shells of variable thickness under a nonstationary load. *International Applied Mechanics*, vol. 50, no. 3, pp. 295–302. DOI: https://doi.org/10.1007/s10778-014-0632-z

6. Dai Q., Cao Q., Chen Y. (2016). Free vibration analysis of truncated circular conical shells with variable thickness using the Haar wavelet method. *Journal of Vibroengineering*, vol. 18, no. 8, pp. 5291–5305. URL: https://www.extrica.com/article/16976

7. Hao Y., Sun L., Zhang W., Li H. (2025). Active traveling wave vibration control of elastic supported conical shells with smart micro fiber composites based on the differential quadrature method. *Applied Mathematics and Mechanics (English Edition),* vol. 46, pp. 305–322. DOI: https://doi.org/10.1007/s10483-025-3216-7

8. Zhao Z., Gao J., Li F., Afshari H. (2026). Frequency and mass optimization for an axially functionally graded GNP-reinforced conical shell with variable thickness. *Applied Mathematics and Mechanics (English Edition), vol*. 47, pp. 859–882. DOI: https://doi.org/10.1007/s10483-026-3373-7

9. Gaidaichuk V., Kotenko K., Mamedov A. (2024). Dynamics of layered conical shells under non-stationary loading. *Strength of Materials and Theory of Structures,* no. 113, pp. 99–107. DOI: https://doi.org/10.32347/2410-2547.2024.113.99-107

10. Khalmuradov R., Khudoynazarov K., Ismoilov K. (2025). Mathematical modelling of torsional vibrations of a truncated conical shell located in an elastic medium. *Engineering Solid Mechanics*, vol. 13, pp. 29–38. DOI: https://doi.org/10.5267/j.esm.2024.9.001